This is a repository copy of *Molecular architecture of the complete COG tethering complex*.

White Rose Research Online URL for this paper:
https://eprints.whiterose.ac.uk/148432/

Version: Accepted Version

Article:

Molecular architecture of the complete COG tethering complex

Jun Yong Ha[1,6], Hui-Ting Chou[2,6], Daniel Ungar[1,3], Calvin K. Yip[2,4], Thomas Walz[2,5], and Frederick M. Hughson[1]

[1]Department of Molecular Biology, Princeton University, Princeton, New Jersey, USA.

[2]Department of Cell Biology, Harvard Medical School, Boston, Massachusetts, USA.

[3]Present Address: Department of Biology, University of York, York, UK.

[4]Present Address: Department of Biochemistry and Molecular Biology, University of British Columbia, Vancouver, Canada

[5]Present Address: The Rockefeller University, New York, New York, USA.

[6]These authors contributed equally to this work.

Correspondence should be addressed to F.M.H. (hughson@princeton.edu) or T.W. (twalz@rockefeller.edu).

Running Title: "Molecular architecture of the COG complex"

Abstract

The conserved oligomeric Golgi (COG) complex orchestrates vesicular trafficking to and within the Golgi apparatus. Here, we use negative-stain electron microscopy to elucidate the architecture of the hetero-octameric COG complex from *Saccharomyces cerevisiae*. Intact COG has an intricate shape, with four (or possibly five) flexible legs, that differs strikingly from the exocyst complex and appears well-suited for vesicle capture and fusion.

Main text

Soluble *N*-ethylmaleimide-sensitive factor attachment protein receptor (SNARE) proteins form membrane-bridging complexes that play a central role in intracellular membrane fusion[1]. The spontaneous assembly of these 'trans' SNARE complexes is, however, inefficient, and is orchestrated *in vivo* by other factors including Sec1/Munc18 (SM) proteins and multisubunit tethering complexes (MTCs)[1,2]. MTCs, containing from three to ten subunits and including the conserved oligomeric Golgi (COG) complex studied here, bridge membranes by binding to lipids, SNAREs, vesicle coat proteins, SM proteins, and/or Rab GTPases – in short, to most of the other proteins implicated in the docking and fusion of a cargo-carrying intracellular trafficking vesicle[2]. Many aspects of MTC structure and mechanism remain, however, to be elucidated.

Five different MTCs, functioning in distinct intracellular trafficking pathways, comprise the CATCHR (Complexes Associated with Tethering Containing Helical Rods) family[2-4]. X-ray structural analysis of individual CATCHR subunits shows that most were likely derived from a common evolutionary progenitor containing α-helical bundle domains arranged in series[5-9]. Many individual CATCHR subunits contain, near their N termini, sequences predicted to form coiled coils, prompting the suggestion that the subunit N termini mediate complex assembly[4]. Two x-ray structures, each containing a pair of interacting CATCHR subunits, are consistent with this hypothesis[8,10].

An improved understanding of CATCHR complex function likely depends on improved characterization of their overall structure. Previously, we reported the essentially complete structure, derived from overlapping crystal structures and negative-stain EM, of the three-subunit Dsl1 complex, which revealed two long, spindly legs with a hinge between them[11]. We have also been studying the more elaborate COG complex, a hetero-octamer. We previously found by negative-stain EM that a core complex (sometimes called lobe A) containing the four subunits Cog1-4 contains three curved legs in a Y-shaped configuration[12]. The remaining four

COG subunits (Cog5-8, sometimes called lobe B) are non-essential in yeast but are the site of many mutations causing congenital disorders of glycosylation (CDG) in humans[12-15]. Here, we present structural analysis of Cog5-8 and of the intact, eight-subunit complex, Cog1-8.

To elucidate the architecture of the COG complex, we used bacterial co-expression of yeast COG subunits. After extensive optimization (see Online Methods for details), we were able to produce the Cog5-8 complex (from the yeast *Kluyveromyces lactis*; Supplementary Fig. 1) and the intact Cog1-8 complex (from *S. cerevisiae*; Fig. 1). Negative-stain EM and class averaging revealed that the *K. lactis* Cog5-8 has an overall rod-like shape, with a length of 27 ± 2 nm and varying degrees of curvature (Supplementary Fig. 1). Most class averages showed evidence of a globular density or hook at one end.

For the intact *S. cerevisiae* COG complex, Cog1-8, we obtained 271 class averages (Supplementary Fig. 2). The overall structure is striking for its lack of compactness, with multiple legs each exhibiting a reproducible curvature (Fig. 1). The relative orientation of the legs varies among the class averages. Although artifacts introduced by deposition and negative staining cannot be ruled out, our findings suggest that Cog1-8 contains flexible hinges as observed for Cog1-4[12] and Cog5-8. The extended structure and apparent flexibility seem well-suited to a role in vesicle capture and SNARE assembly.

Previously, we named the three legs of the Y-shaped Cog1-4 complex A, B, and C, and used GFP tagging of subunit termini to map the locations of the four subunits (Fig. 2a)[12]. We also collected data for Cog1-4+Cog8 and found that Cog8 formed an extension on the end of leg C (Fig. 2a)[12]. The Cog1-4+8 substructure, containing legs A and B and extended leg C, is readily discernable in most class averages of the intact COG complex (Fig. 2a and Supplementary Fig. 2). In addition, Cog1-8 contains a fourth leg, leg D (Fig. 2c). In some class averages, leg D appears to emerge from a triangular junction entailing two distinct points of contact with extended leg C (Fig. 2a).

We next attempted to map the locations of the subunits in the *K. lactis* Cog5-8 complex by fusing GFP to the N and C terminus of each subunit in turn (Supplementary Fig. 3a). (It was not feasible to apply this strategy to the intact Cog1-8 complex, because of its inherent structural variability and hence the need for very large numbers of particles to generate informative class averages.) GFP tags at the C terminus of Cog6, and at both termini of Cog8, were clearly visible in most class averages (Fig. 2b and Supplementary Fig. 3b). GFP tags at the remaining five termini were difficult to discern. Nonetheless, the results showed that the two ends of the rod-like Cog5-8 complex represent the C termini of the two largest subunits, Cog6 and Cog8. Our failure to visualize an N-terminal GFP tag on Cog6 (Supplementary Fig. 3b), together with the ability of N-terminally truncated Cog6(Δ1-146) to form Cog5-8 complexes, led us to speculate that the N terminus might be flexible. Therefore, we prepared complexes containing GFP attached to the truncated N terminus of Cog6. In these samples, the GFP tag was clearly visible (Fig. 2b and Supplementary Fig. 3b). Further attempts to locate the termini of Cog5 and Cog7 (e.g., via MBP labeling) were unsuccessful, suggesting that, at least in the Cog5-8 complex, they are too flexible.

Given the known location of Cog8 relative to Cog1-4, the length of the *K. lactis* Cog5-8 complex, and the fact that *S. cerevisiae* Cog8 is approximately twice as large as *K. lactis* Cog8, it was straightforward to place Cog6 and Cog8 within the full *S. cerevisiae* Cog1-8 complex (Fig. 2c and Supplementary Fig. 4). This analysis revealed that the C terminus of Cog8 represents the distal tip of extended leg C, while the C terminus of Cog6 represents the distal tip of the newly discovered leg D. Like the other legs, leg D has a width of approximately 3 nm, consistent with the conserved CATCHR fold.

The C termini of the four largest *S. cerevisiae* subunits (Cog3, 4, 6, and 8) represent the distal tips of legs A, B, D, and C, respectively. Because the legs adopt different positions in different class averages, the inter-leg distance varies dramatically (Fig. 1 and Supplementary

Movie 1). In some class averages, the distal tip of leg B can be 14 nm or more away from leg C, whereas in other class averages it appears to make direct contact (Fig. 1). This may be a deposition artifact; alternatively, it may indicate a low affinity interaction between the tip of leg B and leg C. Interestingly, a mutation that destabilizes the tip of leg B causes a CDG in humans[7,16]. Meanwhile, the distance between distal tips of legs A and D varies from 7 to 38 nm (Fig. 1).

We were unable to locate Cog5 and Cog7 within the Cog5-8 complex. However, a previous crystal structure of a complex between Cog5 and Cog7 revealed that they interact via antiparallel α-helices near their N termini[10]. Intriguingly, in about 10% of the Cog1-8 class averages, a fifth leg can be discerned (Fig. 2d). This leg presumably contains Cog5 and/or Cog7, with one of the two C termini at its distal tip. We call this leg E′, with the prime denoting our remaining uncertainty about its composition (Fig. 2d).

Since COG is conserved from yeast to mammals, we used negative-stain EM to examine purified bovine COG[17]. The particles were too heterogeneous for class averaging, and many gave the impression of being self-entangled (Fig. 2e and Supplementary Fig. 5). Nonetheless, Fig. 2e highlights a single, albeit non-representative, particle with a striking resemblance to *S. cerevisiae* COG. Extra densities in the middle of leg C (blue arrow) are presumably attributable to the greater size of bovine (compared to yeast) Cog1 and/or Cog2. Similarly, bovine Cog5 and Cog7 are much larger than their yeast orthologs, providing a plausible explanation for additional densities near the Cog1–Cog8 junction (red circle). We provisionally conclude that the overall architecture of COG is conserved from yeast to mammals.

The known CATCHR complexes have three (Dsl1), four (GARP and EARP), or eight (COG and exocyst) subunits. It might have been anticipated that COG and exocyst would resemble one another; instead, they are strikingly different. Recent negative-stain EM of the yeast exocyst complex revealed a compact bundle of rods, proposed to represent individual exocyst subunits

arranged roughly in parallel[18]. By contrast, the known subunit-subunit interactions in COG involve antiparallel interactions between N-terminal regions (Fig. 2b and refs. 10 and 12). Perhaps this difference – parallel versus antiparallel subunit interactions – underpins the dramatically contrasting overall architectures of the two complexes, which in any case calls into question the assumption that the COG and exocyst complexes have similar mechanisms of action.

COG is remarkable for the number of interactions it apparently has with Golgi SNARE proteins, Rab GTPases, coat proteins and coiled-coil tethers (Supplementary Table 1)[14]. Our structural results should provide a useful foundation for mapping out the geometrical relationships between these binding sites and, ultimately, their mechanistic significance.

Acknowledgements

Author Contributions

All authors designed experiments and analyzed data. J.Y.H., H.-T.C., D.U., and C.K.Y. performed the experiments. J.Y.H., H.-T.C., T.W., and F.M.H. wrote the manuscript.

Competing Financial Interests Statement

The authors declare no competing financial interests.

References

1.   Südhof, T.C. & Rothman, J.E. Membrane fusion: grappling with SNARE and SM proteins. *Science* **323**, 474-477 (2009).

2.   Yu, I.M. & Hughson, F.M. Tethering factors as organizers of intracellular vesicular traffic. *Annu Rev Cell Dev Biol* **26**, 137-56 (2010).

3.   Schindler, C., Chen, Y., Pu, J., Guo, X. & Bonifacino, J.S. EARP is a multisubunit tethering complex involved in endocytic recycling. *Nat Cell Biol* **17**, 639-50 (2015).

4.   Whyte, J.R. & Munro, S. Vesicle tethering complexes in membrane traffic. *J Cell Sci* **115**, 2627-2637 (2002).

5.   Dong, G., Hutagalung, A.H., Fu, C., Novick, P. & Reinisch, K.M. The structures of exocyst subunit Exo70p and the Exo84p C-terminal domains reveal a common motif. *Nat Struct Mol Biol* **12**, 1094-1100 (2005).

6.   Perez-Victoria, F.J. et al. Structural basis for the wobbler mouse neurodegenerative disorder caused by mutation in the Vps54 subunit of the GARP complex. *Proc Natl Acad Sci U S A* **107**, 12860-5 (2010).

7.   Richardson, B.C. et al. Structural basis for a human glycosylation disorder caused by mutation of the COG4 gene. *Proc Natl Acad Sci U S A* **106**, 13329-34 (2009).

8.   Tripathi, A., Ren, Y., Jeffrey, P.D. & Hughson, F.M. Structural characterization of Tip20p and Dsl1p, subunits of the Dsl1p vesicle tethering complex. *Nat Struct Mol Biol* **16**, 114-23 (2009).

9.   Vasan, N., Hutagalung, A., Novick, P. & Reinisch, K.M. Structure of a C-terminal fragment of its Vps53 subunit suggests similarity of Golgi-associated retrograde protein (GARP) complex to a family of tethering complexes. *Proc Natl Acad Sci U S A* **107**, 14176-81 (2010).

10.   Ha, J.Y. et al. Cog5-Cog7 crystal structure reveals interactions essential for the function of a multisubunit tethering complex. *Proc Natl Acad Sci U S A* **111**, 15762-7 (2014).

11.   Ren, Y. et al. A structure-based mechanism for vesicle capture by the multisubunit tethering complex Dsl1. *Cell* **139**, 1119-29 (2009).

12.   Lees, J.A., Yip, C.K., Walz, T. & Hughson, F.M. Molecular organization of the COG vesicle tethering complex. *Nat Struct Mol Biol* **17**, 1292-7 (2010).

13.   Freeze, H.H. & Ng, B.G. Golgi glycosylation and human inherited diseases. *Cold Spring Harb Perspect Biol* **3**, a005371 (2011).

14.   Willett, R., Ungar, D. & Lupashin, V. The Golgi puppet master: COG complex at center stage of membrane trafficking interactions. *Histochem Cell Biol* **140**, 271-83 (2013).

15.   Miller, V.J. & Ungar, D. Re'COG'nition at the Golgi. *Traffic* **13**, 891-7 (2012).

16.   Reynders, E. et al. Golgi function and dysfunction in the first COG4-deficient CDG type II patient. *Hum Mol Genet* **18**, 3244-56 (2009).

17.   Ungar, D. et al. Characterization of a mammalian Golgi-localized protein complex, COG, that is required for normal Golgi morphology and function. *J Cell Biol* **157**, 405-415 (2002).

18.   Heider, M.R. et al. Subunit connectivity, assembly determinants and architecture of the yeast exocyst complex. *Nat Struct Mol Biol* **23**, 59-66 (2016).

19.   Lübbehusen, J. et al. Fatal outcome due to deficiency of subunit 6 of the conserved oligomeric Golgi complex leading to a new type of congenital disorders of glycosylation. *Hum Mol Genet* **19**, 3623-33 (2010).

20.   Foulquier, F. et al. A new inborn error of glycosylation due to a Cog8 deficiency reveals a critical role for the Cog1-Cog8 interaction in COG complex formation. *Hum Mol Genet* **16**, 717-30 (2007).

Figure Legends

Figure 1. Purification and negative-stain EM of the yeast COG complex. At the left is the purified *S. cerevisiae* Cog1-8 complex visualized by SDS-PAGE and Coomassie Blue staining. At the right are a representative image field and a gallery of class averages (see also Supplementary Fig. 2). The uncropped gel image is shown in Supplementary Data Set 1.

Figure 2. Molecular architecture of the COG complex. (**a**) *S. cerevisiae* Cog1-4[12], Cog1-4+8 (bearing an N-terminal GFP tag on Cog4)[12], and Cog1-8. Cog1-4 and Cog1-4+8 adapted from ref. 12, Nature Publishing Group. (**b**) Localization of GFP tags from *K. lactis* Cog5-8 complexes (see also Supplementary Fig. 3). GFP-Cog6ΔN represents GFP attached to the N terminus of Cog6 (residues 147-779). (**c**) Model for subunit organization of the fully assembled COG complex (see also Supplementary Fig. 4). The positions of Cog5 and Cog7 were not determined in this study. X's denote the approximate positions of selected CDG mutations in human Cog4 (R729W)[16], Cog6 (G549V)[19], and Cog8 (Y537X)[20]. (**d**) Representative class averages displaying leg E′ (yellow arrows). (**e**) An image field of bovine COG (see also Supplementary Fig. 5), as well as a single particle shown at higher magnification. On the right, for comparison, is a representative class average for yeast COG. See text for further details.

Online Methods

Plasmid construction and protein purification

We initially attempted to co-express *S. cerevisiae* Cog5, Cog6, Cog7, and Cog8 (Cog5-8) using the pQLink vector system in *Escherichia coli*; however, the levels of Cog6 protein were undetectably low. As an alternative, we switched to *Kluyveromyces lactis*. The four coding sequences, inserted into pQLinkH, were co-expressed in *E. coli* BL21-CodonPlus(DE3)-RIPL cells (Agilent Technologies). Cog6 contained an N-terminal His_6 tag. Cells were grown at 37°C to an OD_{600} of approximately 0.6-0.8 in LB medium containing 100 μg/ml ampicillin. Protein expression was induced using 0.5 mM isopropyl β-D-1-thiogalactopyranoside (IPTG). The growth temperature was then lowered to 18°C and cells were grown for 12-18 h before harvesting. Cell pellets were resuspended in lysis buffer (20 mM Tris-HCl, pH 8.0, 150 mM NaCl, 5% glycerol, 1 mM phenylmethanesulfonyl fluoride (PMSF), 0.25 tablet of EDTA-free protease inhibitor cocktail (Sigma-Aldrich) per liter of bacterial culture, 2 μg/mL DNase I) and lysed using a cell disruptor (Avestin). The Cog5-8 complex was purified using affinity (Ni^{2+}-NTA; Clontech), anion exchange (MonoQ; GE Healthcare), and size-exclusion (Superdex 200; GE Healthcare) chromatography and stored in storage buffer (20 mM Tris, pH 8.0, 150 mM NaCl, 1 mM dithiothreitol, 1 mM EDTA, 0.2 mM PMSF and 1 tablet per liter EDTA-free protease inhibitor cocktail). We also constructed nine additional vectors, each encoding a single GFP-tagged subunit and three untagged subunits. The GFP tags were placed at the N and C termini of each subunit; in the ninth vector, the GFP tag was placed at the N terminus of a truncated *COG6* gene encoding Cog6 without its first 146 residues, Cog6ΔN. The corresponding GFP-tagged Cog5-8 complexes were purified as described above (Supplementary Fig. 3a). Cog5-8 complexes with N- and C-terminal GFP tags on Cog6 were His_6-tagged at the C terminus of Cog6 and the N terminus of Cog7, respectively; all other GFP-tagged Cog5-8 complexes were (like untagged Cog5-8) His_6-tagged at the N terminus of Cog6.

Extensive efforts were made to isolate the fully assembled hetero-octameric COG complex. First, we prepared two pQLinkH plasmids containing either all eight *K. lactis COG* genes or all eight *S. cerevisiae COG* genes. In neither case, however, we were able to isolate the intact COG complex. We next sought to overproduce *K. lactis* Cog1-4 according to the same strategy, with the idea of combining it with *K. lactis* Cog5-8, but found that Cog4 was insoluble when overproduced in bacteria. As a final approach, we sought to overcome our above-mentioned difficulty in producing *S. cerevisiae* Cog5-8 – that is, that Cog6 was not expressed at detectable levels – reasoning that this might allow us to combine *S. cerevisiae* Cog5-8 with *S. cerevisiae* Cog1-4, the subject of an earlier study[12]. To increase the expression level of *S. cerevisiae* Cog6, we had the corresponding gene synthesized (GENEWIZ) using codons optimized for bacterial expression and reinserted it into the pQLinkH vector. Co-expression with *S. cerevisiae* Cog5, Cog7, and Cog8 yielded small amounts of the *S. cerevisiae* Cog5-8 complex, although the Cog6 protein was partially degraded during purification. This degradation problem was alleviated by co-lysing cell pellets containing the *S. cerevisiae* Cog1-4 and Cog5-8 subassemblies, enabling us to purify fully assembled Cog1-8. Specifically, Cog1-4 containing N-terminally His_6-tagged Cog2 was overproduced in C43(DE3) (Lucigen), while Cog5-8 containing N-terminally His_6-tagged Cog6 was overproduced in BL21-CodonPlus(DE3)-RIPL cells (Agilent Technologies). After growing cells at 37°C to an OD_{600} of approximately 0.6-0.8 in LB medium containing 100 μg/ml ampicillin, the cells containing Cog1-4 and Cog5-8 were induced at 23 and 18°C, respectively, with 0.5 mM IPTG and grown an additional 12-18 h. After harvesting, the cells were resuspended in lysis buffer, combined, lysed using a cell disruptor, and purified as described above for *K. lactis* Cog5-8.

Bovine COG was purified as previously described[17].

Electron microscopy and image processing

To prepare negatively stained grids, 3 μl sample was added to a glow-discharged carbon-coated grid and stained with 2% uranyl formate as described[21]. The grids were imaged with an FEI Tecnai T12 electron microscope operated at 120 kV at a defocus of −1.5 μm using low-dose procedures. Images were acquired at a nominal magnification of 42,000x using a Gatan 4K x 4K CCD camera, which gave a calibrated pixel size of 2.61 Å on the specimen level. Particles were picked with e2boxer.py[22], windowed into 145 x 145-pixel images (all Cog5-8 complexes) or 240 x 240-pixel images (Cog1-8 complex), and normalized. The images were reduced to 64 x 64 pixels, and the particles were centered and then classified using the Iterative Stable Alignment and Clustering (ISAC) procedure[23].

For *S. cerevisiae* Cog1-8 (total of 31,872 particles), 18 ISAC generations with 100 particles per group and a pixel error threshold of 2 yielded 271 classes (Supplementary Fig. 2), accounting for 5,182 particles (~16% of the entire data set).

For untagged *K. lactis* Cog5-8 (total of 8,825 particles), 14 ISAC generations with 200 particles per group and a pixel error threshold of 2 yielded 129 classes (Supplementary Fig. 1b), accounting for 4,958 particles (~56% of the entire data set).

Data were also collected for nine GFP-tagged *K. lactis* Cog5-8 complexes (Supplementary Fig. 3a). It proved possible to locate GFP in class averages of *K. lactis* Cog5-8 complexes containing GFP attached to: (1) the N terminus of Cog6ΔN, (2) the C terminus of full-length Cog6, (3) the N terminus of Cog8, and (4) the C terminus of Cog8 (Supplementary Fig. 3b). For Cog5-8 containing N-terminally GFP-tagged Cog6ΔN (total of 5,689 particles), 3 ISAC generations with 50 particles per group and a pixel error threshold of 0.7 yielded 73 classes, accounting for 1,189 particles (~21% of the entire data set). For Cog5-8 with C-terminally GFP-tagged Cog6 (total of 6,412 particles), 4 ISAC generations with 100 particles per group and a pixel error threshold of 0.7 yielded 125 classes, accounting for 3,109 particles (~48% of the entire data set). For Cog5-8 with N-terminally GFP-tagged Cog8 (total of 7,237 particles), 14

ISAC generations with 200 particles per group and a pixel error threshold of 2 yielded 72 classes, accounting for 2,434 particles (~34% of the entire data set). For Cog5-8 with C-terminally GFP-tagged Cog8 (total of 8,247 particles), 8 ISAC generations with 200 particles per group and a pixel error threshold of 2 yielded 97 classes, accounting for 4,185 particles (~51% of the entire data set).
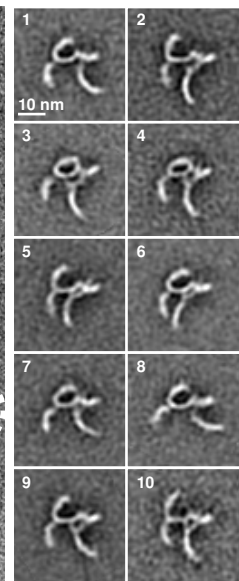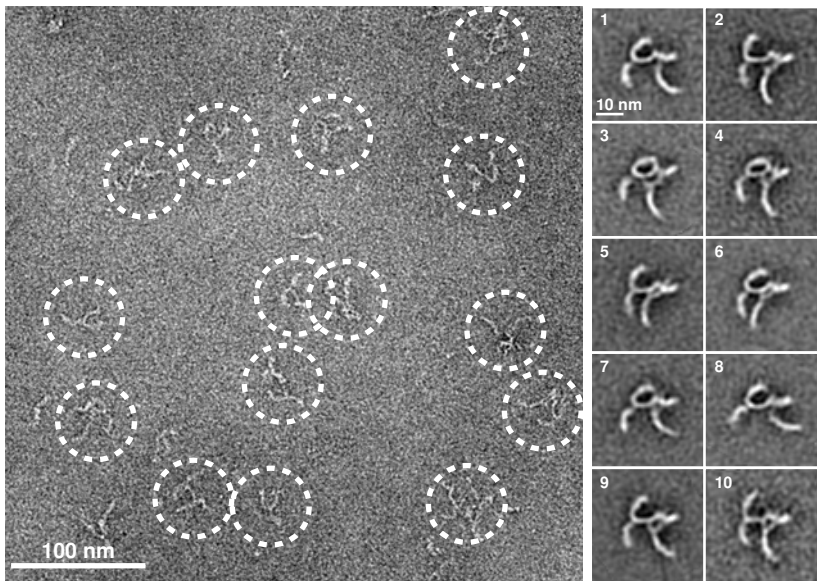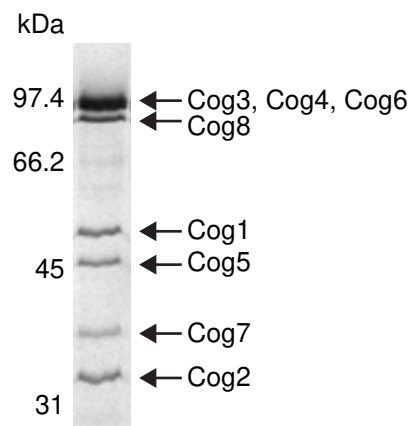
For the other five GFP-tagged *K. lactis* Cog5-8 complexes, class averages did not allow the GFP to be localized (Supplementary Fig. 3b and data not shown). For Cog5-8 with N-terminally GFP-tagged Cog5 (total of 11,380 particles), 3 ISAC classifications with 100 particles per group and a pixel error threshold of 0.7 yielded 137 classes, accounting for 3,012 particles (~26% of the entire dataset). For Cog5-8 with C-terminally GFP-tagged Cog5 (total of 11,477 particles), ISAC classifications with 50 particles per group and a pixel error threshold of 2 yielded 225 classes, accounting for 4,431 particles (~39% of the entire dataset). For Cog5-8 with N-terminally GFP-tagged Cog6 (total of 7,645 particles), ISAC classifications with 100 particles per group and a pixel error threshold of 0.7 yielded 155 classes, accounting for 4,616 particles (~60% of the entire dataset; Supplementary Fig. 3b). For Cog5-8 with N-terminally GFP-tagged Cog7 (total of 10,494 particles), ISAC classifications with 100 particles per group and a pixel error threshold of 0.7 yielded 181 classes, accounting for 3,797 particles (~36% of the entire dataset). For Cog5-8 with C-terminally GFP-tagged Cog7 (total of 9,997 particles), ISAC classifications with 50 particles per group and a pixel error threshold of 2 yielded 257 classes, accounting for 4,163 particles (~44% of the entire dataset).
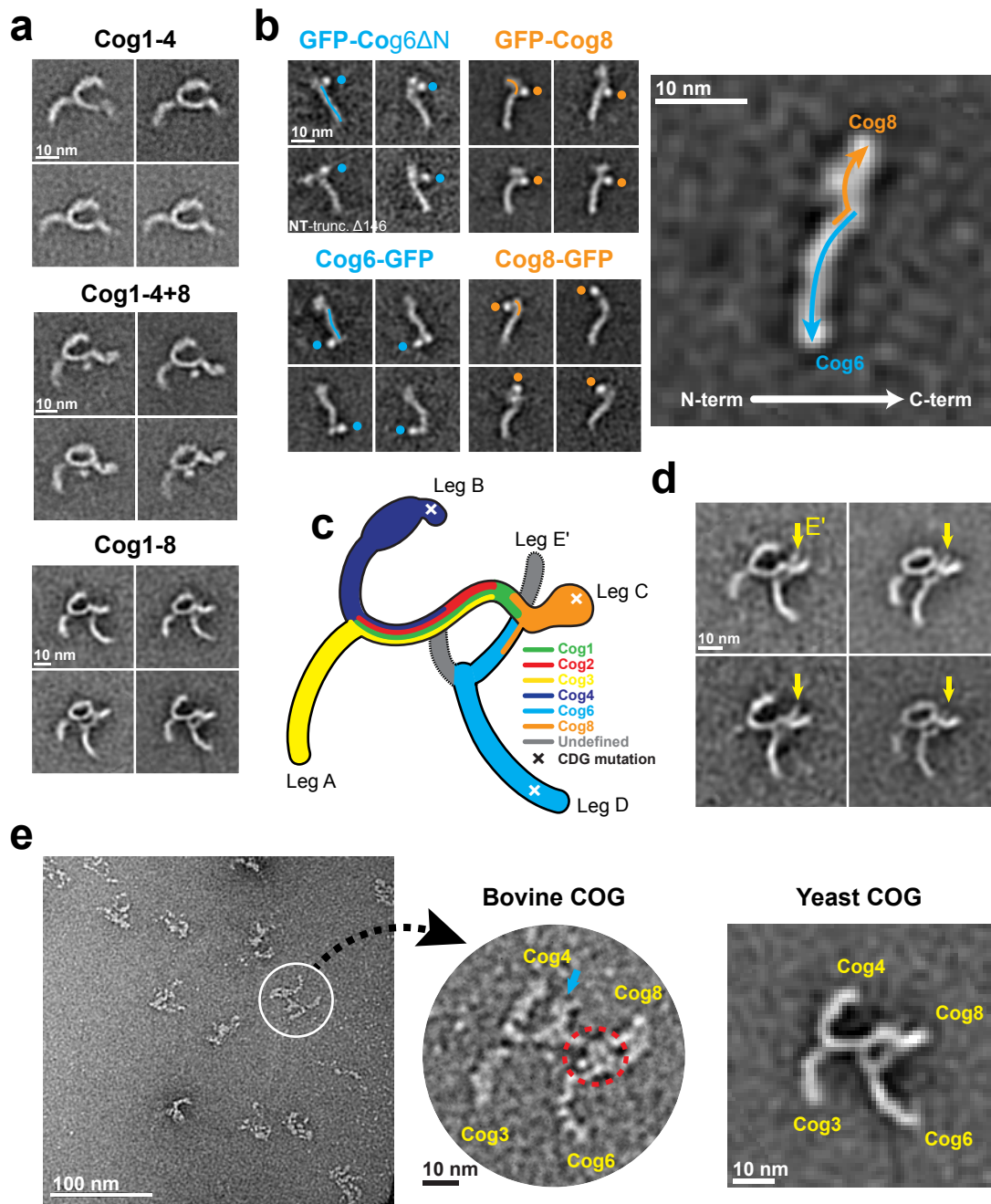
Methods-Only References

21. Ohi, M., Li, Y., Cheng, Y. & Walz, T. Negative staining and image classification - powerful tools in modern electron microscopy. *Biol Proced Online* **6**, 23-34 (2004).

22.   Tang, G. et al. EMAN2: an extensible image processing suite for electron microscopy. *J Struct Biol* **157**, 38-46 (2007).

23.   Yang, Z., Fang, J., Chittuluru, J., Asturias, F.J. & Penczek, P.A. Iterative stable alignment and clustering of 2D transmission electron microscope images. *Structure* **20**, 237-47 (2012).

a

Cog1-4

10 nm

Cog1-4+8

10 nm

Cog1-8

10 nm

b

GFP-Cog6ΔN   GFP-Cog8

10 nm

NT-trunc. Δ146

Cog6-GFP   Cog8-GFP

10 nm

Cog8

Cog6

N-term ➝ C-term

c

Leg B

Leg E'

Leg C

Cog1
Cog2
Cog3
Cog4
Cog6
Cog8
Undefined
CDG mutation

Leg A

Leg D

d

E'

10 nm

e

100 nm

Bovine COG

Cog4
Cog8
Cog3
Cog6

10 nm

Yeast COG

Cog4
Cog8
Cog3
Cog6

10 nm

Supplementary Table 1. Yeast COG interactome.

COG subunit	Partner	Class	Reference
Cog1	COPI	Coat	1
Cog2	Sed5	SNARE	1
	Ypt1	Rab	1
	Ypt6	Rab	1
	COPI	Coat	1
	Sec21	Coat	1
Cog3	Sed5	SNARE	1
	Ykt6	SNARE	1
	Gos1	SNARE	1
	Sec22	SNARE	1
	Ypt1	Rab	1
	Ypt6	Rab	1
	Vps52	Tether	2
	COPI	Coat	1
Cog4	Sed5	SNARE	3
	Tip20	Tether	4
	COPI	Coat	1
Cog6	Ypt1	Rab	5
	Ypt6	Rab	5
	COPI	Coat	1

1. Suvorova, E.S., Duden, R. & Lupashin, V.V. The Sec34/Sec35p complex, a Ypt1p effector required for retrograde intra-Golgi trafficking, interacts with Golgi SNAREs and COPI vesicle coat proteins. *J Cell Biol* **157**, 631-43 (2002).

2. Tarassov, K. et al. An in vivo map of the yeast protein interactome. *Science* **320**, 1465-70 (2008).

3. Shestakova, A., Suvorova, E., Pavliv, O., Khaidakova, G. & Lupashin, V. Interaction of the conserved oligomeric Golgi complex with t-SNARE Syntaxin5a/Sed5 enhances intra-Golgi SNARE complex stability. *J Cell Biol* **179**, 1179-1192 (2007).

4. Uetz, P. et al. A comprehensive analysis of protein-protein interactions in *Saccharomyces cerevisiae. Nature* **403**, 623-7 (2000).

5. Yu, H. et al. High-quality binary protein interaction map of the yeast interactome network. *Science* **322**, 104-10 (2008).
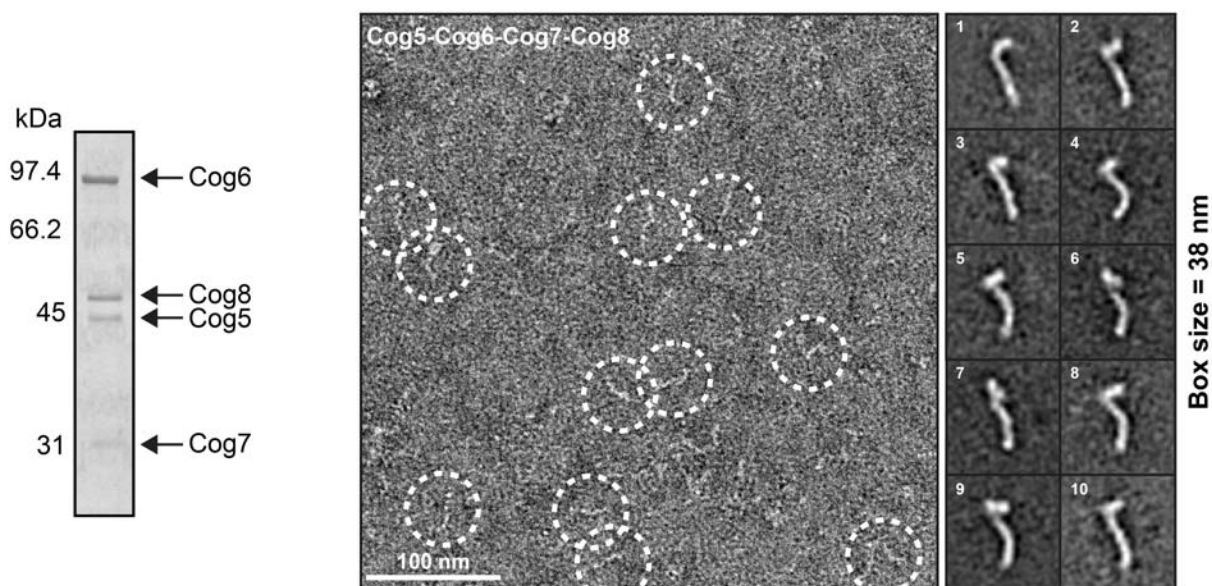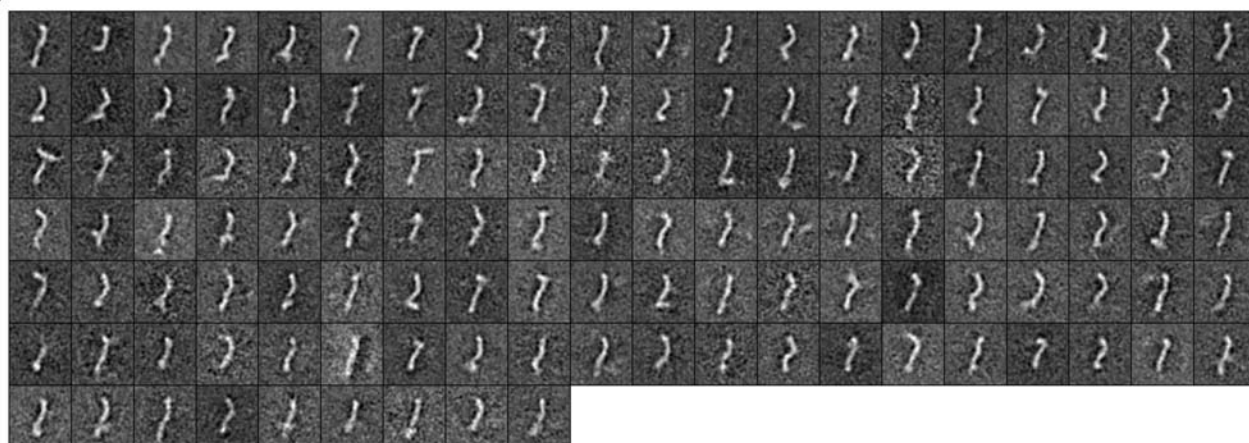
Supplementary Figure 1

Purification and negative-stain EM of *K. lactis* Cog5-8.

(**a**) The purified recombinant *K. lactis* Cog5-8 complex, visualized by SDS-PAGE and Coomassie Blue staining, is shown together with a representative image field and ten representative class averages. (**b**) Complete gallery of *K. lactis* Cog5-8 class averages (side length of each panel = 38 nm). The 129 class averages, which account for 4,958 particles, were obtained by subjecting 8,825 particles to 14 generations of ISAC.
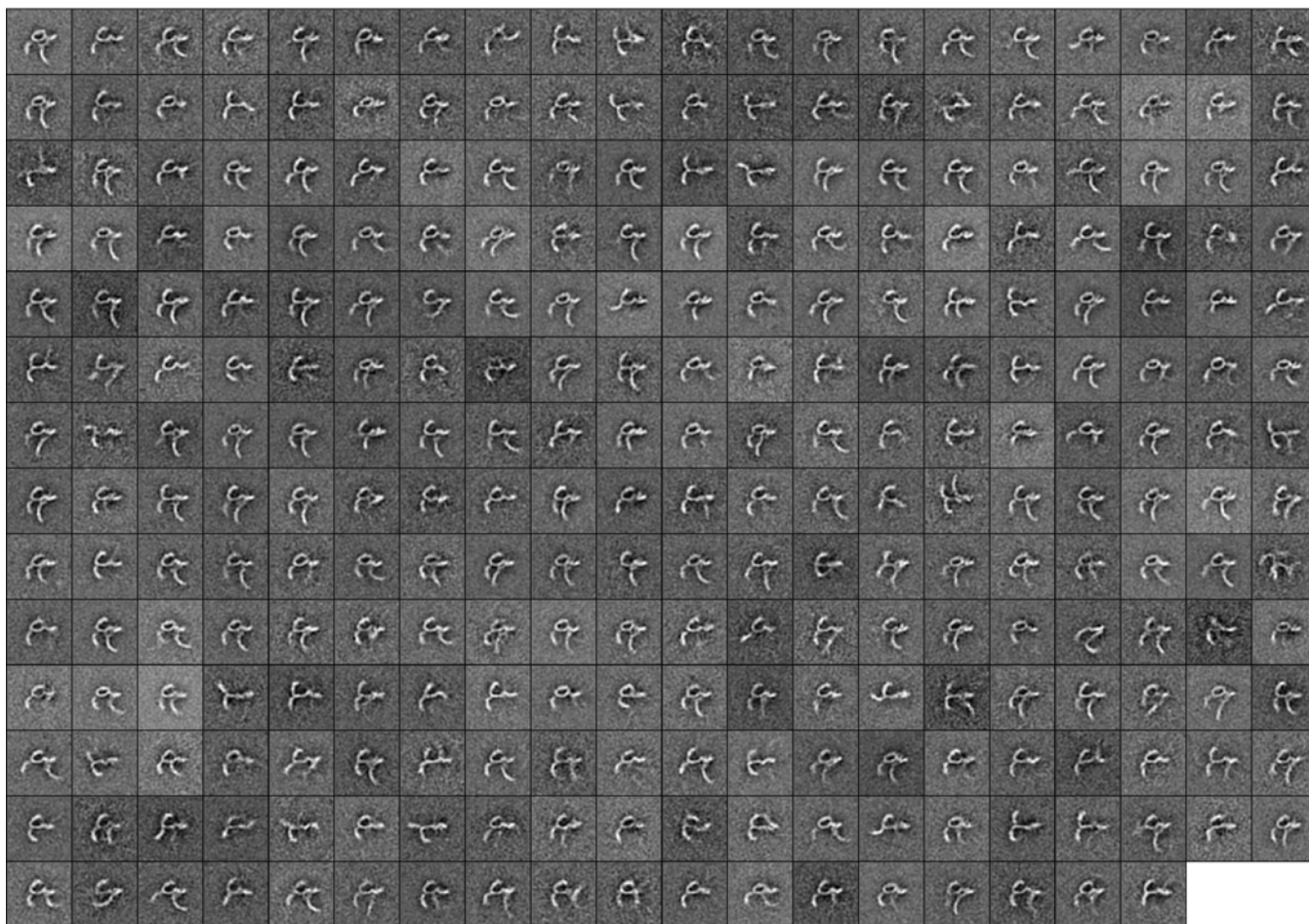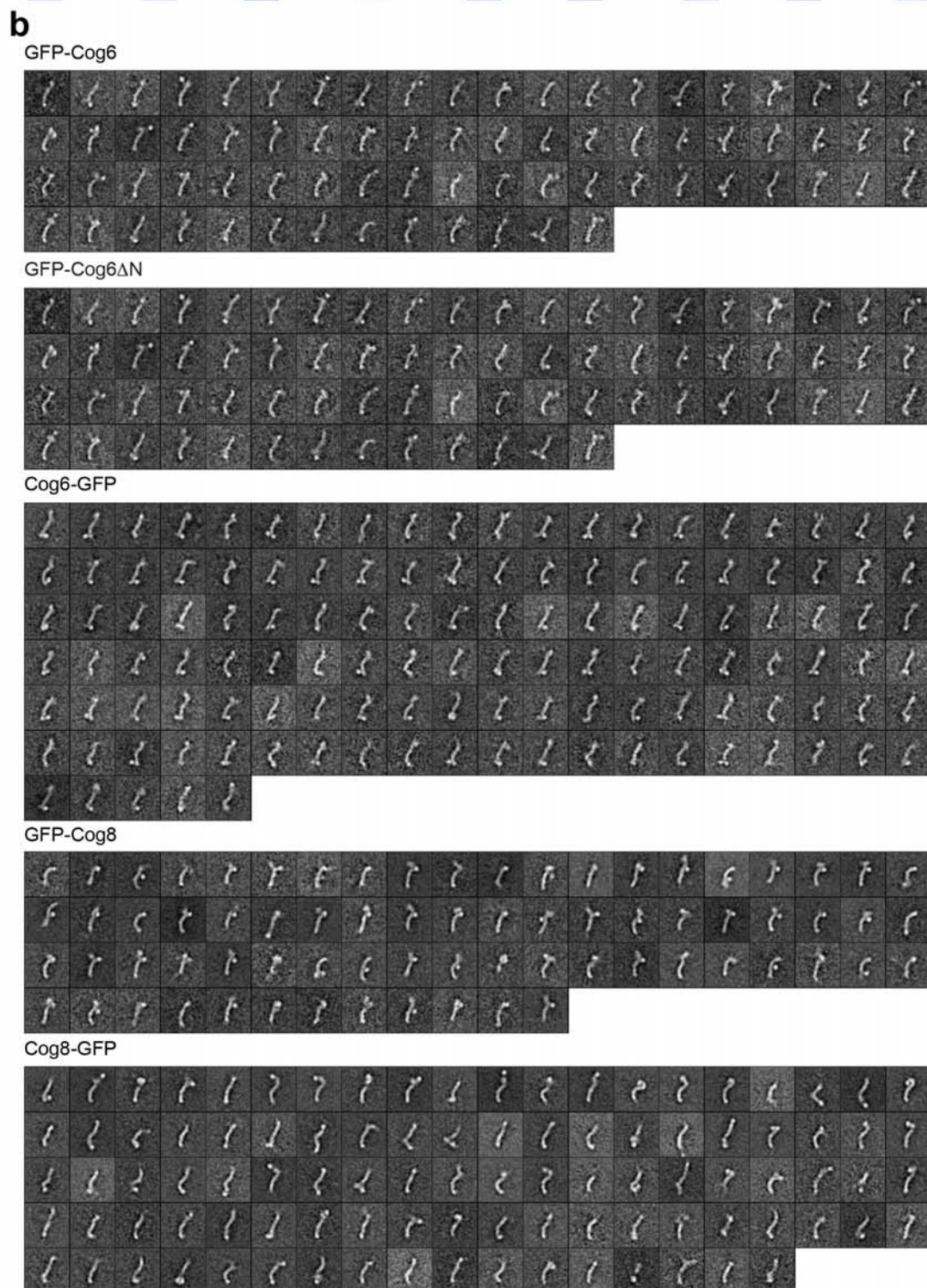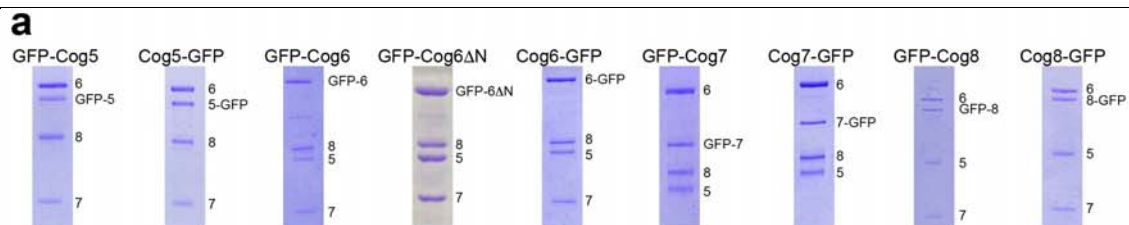
Supplementary Figure 2

Negative-stain EM of *S. cerevisiae* Cog1-8.

Complete gallery of *S. cerevisiae* Cog1-8 class averages (side length of each panel = 63 nm). The 271 class averages, which account for 5,182 particles, were obtained by subjecting 31,872 particles to 18 generations of ISAC.

a

GFP-Cog5   Cog5-GFP   GFP-Cog6   GFP-Cog6ΔN   Cog6-GFP   GFP-Cog7   Cog7-GFP   GFP-Cog8   Cog8-GFP

b

GFP-Cog6

GFP-Cog6ΔN

Cog6-GFP

GFP-Cog8

Cog8-GFP

Supplementary Figure 3

Localizing individual subunits within the *K. lactis* Cog5-8 complex.

(**a**) Purified *K. lactis* Cog5-8 complexes containing single GFP tags, visualized by SDS-PAGE and Coomassie Blue staining. GFP-Cog6ΔN denotes N-terminally truncated Cog6 (residues 147-779). (**b**) Complete galleries of GFP-tagged *K. lactis* Cog5-8 class averages (side length of each panel = 38 nm). Only those complexes in which the GFP tag was visible in class averages are included; the remaining complexes were indistinguishable from the untagged complexes shown in Supplementary Fig. 1b.
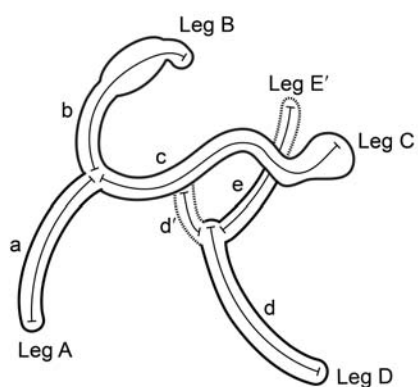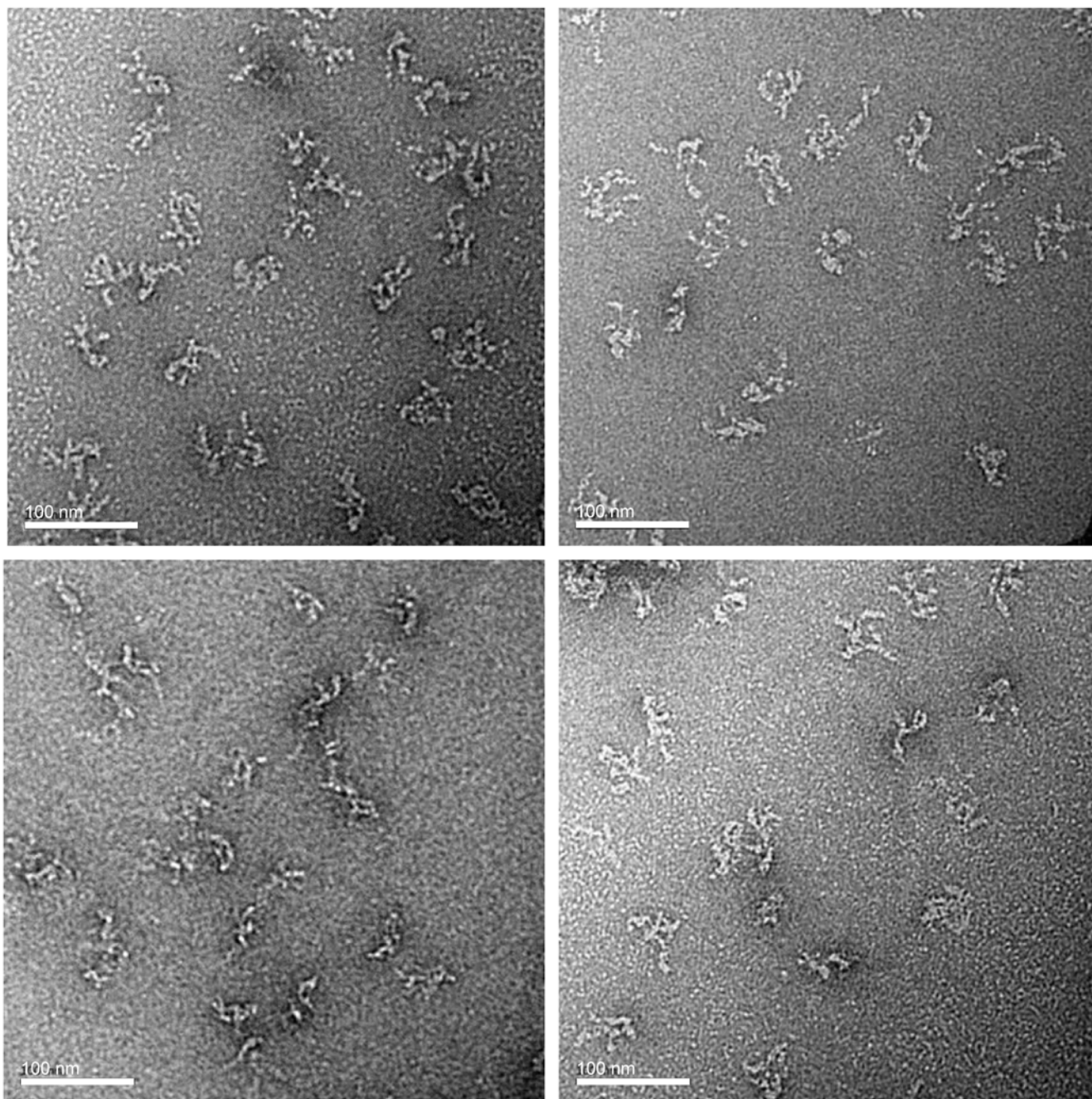
Structural element	Length (nm)
a	17.9 ± 0.8
b	18.7 ± 0.9
c	27.0 ± 0.5
d	21.7 ± 0.9
d′	5.7 ± 0.7
e	12.6 ± 1.1

Supplementary Figure 4

Dimensions of *S. cerevisiae* Cog1-8.

The indicated lengths (mean ± s.d.; n=5) were derived from class averages using ImageJ (https://imagej.nih.gov/ij/).

Supplementary Figure 5

Negative-stain EM of bovine COG.

Shown are four additional image fields of the bovine COG complex (see also Fig. 2e). The particles were too heterogeneous to allow successful class averaging.

Supplementary Data Set 1. Uncropped gel for Figure 1

Size exclusion chromatography for COG complex in Figure 1

Cropped box shown in Figure 1
(This fraction was used for collecting EM data)